Chapter 5

Switched Reluctance Drives with Degraded Mode for Electric Vehicles

Pablo Moreno-Torres, Marcos Lafoz, Marcos Blanco,
Gustavo Navarro, Jorge Torres and
Luis García-Tabarés

Additional information is available at the end of the chapter

http://dx.doi.org/10.5772/64431

Abstract

There are many types of electrical machines suitable for electric vehicles. Nowadays, most manufacturers and researchers tend towards two major alternatives: permanent magnet synchronous machines and induction machines. However, these are not the only competitive candidates. Reluctance machines, which have been well-known for some decades already, present some interesting advantages. For instance, switched reluctance machines are intrinsically redundant and fault-tolerant, which makes them attractive for applications in which robustness is compulsory. In this sense, switched reluctance drives can keep working even when one of their phases loses its functionality for any reason. In an electric vehicle, this would mean being able to keep driving the vehicle even after some failures, although with reduced performance (in degraded mode). In this chapter, switched reluctance drives for traction applications are analyzed, focusing on their capability to operate in degraded mode (with m-1 phases available).

Keywords: switched reluctance machine, traction drive, fault-tolerant drive, degraded mode

1. Introduction

In electric vehicles (EVs), the component responsible for providing mechanical torque is the motor. The main requirements for EV motors are high peak power, power density, compactness, high torque over a wide speed range, fast torque response, energy efficiency, reliability, robustness, fault tolerance, low maintenance and low cost [1].

Various motors have been considered for EV applications [2]: DC machines, induction machines (IMs), permanent magnet synchronous machines (PMSM) and switched reluctance machines (SRMs). DC machines are not used any more due to the high maintenance required and the lack of reliability associated to the commutator and the brushes. IMs, commonly used in industrial applications, are a robust option with more reliability and better efficiency than DC machines. However, they present a clear disadvantage which is the heat produced by the losses in the rotor, difficult to extract, requiring a special cooling system and reducing the overload capacity of the motor. PMSMs, and particularly Interior PMSMs (IPMSMs), are the most popular choice for EVs [3, 4]. These motors have higher efficiency, compactness, high-power density, fast dynamics and high torque-to-inertia ratio. However, they show some drawbacks due to the presence of rare earth permanent magnets. The price and the availability of rare earth material are considered a potential problem for EVs massive development [5]. Besides, PMSMs are more sensitive to high temperatures, and they suffer from risk of demagnetization.

Switched reluctance drives (SRDs) are getting increased attention recently, including in the EV industry [6]. SRMs have been well known for many years due to its simple operation principle. Relatively, advances in static switches and digital control devices have fostered its applications in many different fields, even replacing other types of electrical machines.

2. State of the art

A rotary switched reluctance machine consists of a stator, in which an even number of coils are placed in an laminated iron yoke, and a rotor, which comprises only a laminated iron yoke with no coils. Both parts have a polar configuration with different number of poles in each one. Only a restricted combination of pole number for rotor and stator is allowed to run the machine properly. The name of this type of machine comes from the fact that every time a coil is activated, the rotor moves trying to align one of its poles with the corresponding stator one, minimizing the overall reluctance of the magnetic circuit. The SRM is based on the concept of switching the stator coils sequentially. If the coil is switched on before the closest rotor pole is aligned with the active stator one, then the machine acts as a motor, while if it is switched after, then it acts as a generator.

Structural simplicity, high efficiency compared with the induction motor, low cost and control flexibility, rugged motor construction, large starting torque, wide speed range, inherent fault-tolerance capability, and high operating efficiency are some of the characteristics that make the SRM a remarkable candidate for electric drive of electric vehicles and hybrid electric vehicles (HEVs) [7]. The authors of [2] also refer to the SRM suitability for high-speed applications as well as for harsh environment such as EVs, considering high temperature and vibrations. Another important advantage of SRMs is their intrinsic fault tolerance, in the sense that they will continue to operate in a satisfactory manner, without the other phases being affected, after sustaining some types of faults [8]. Moreover, most SRMs can operate even if one of the phases is broken down (degraded mode or “m-1phases” mode), which means that

http://dx.doi.org/10.5772/64431

they are intrinsically redundant [9–11]. Consequently, the SRM combines many desirable qualities of induction machines as well as PM brushless machines. Its performance and inherently low manufacturing cost make it a competitive option for this application.

On the other hand, SRMs have also some disadvantages, such as lower specific torque, high-torque ripple, low efficiency compared with IPMSM and high noise and vibrations [12]. Most authors claim that PMSMs can reach up to twice the power density of SRMs. However, this is only true when the comparison is done in unfair terms: PMSMs are not fault tolerant by default, but they must be for some applications. The good news is that they can be designed to be fault tolerant (although not for high-speed applications); the bad news is that doing so decreases their power density significantly [8]. Besides, PMSM lose torque capability with temperature due to permanent magnets flux reduction [13], much more than SRMs and IMs. As high temperatures could become a common requirement for electric motors in EVs, this fact will further reduce the difference between PMSMs and the other two alternatives. After considering these two points, PMSMs could achieve "only" 25–50% more power density than SRMs [8].

Having a SRM with a higher number of rotor poles than stator poles results in higher efficiency and torque to weight ratio [14, 15]. This is particularly convenient for outer-rotor machines, usually used in in-wheel designs. In such case, a better performance is achieved if a segmented rotor topology is used [16]. Segmented rotor SRMs have a stator with full pitch coils and a rotor with discrete segments embedded in nonmagnetic material.

Regarding torque ripple, several alternatives related to rotor geometry have been extensively studied [17], based on slanting, serration, chamfering or skewing, demonstrating a certain improvement in torque ripple. Other studies have been accomplished varying yoke thickness, stator pole width, internal stator diameter [17, 18] and pole shapes [19].

Various SRM have been designed and built during the last two decades for EV and HEV applications; examples are found in [11, 20–27]. The key points to improve a SRM efficiency are to increase the number of stator and rotor poles, reduce iron losses using 0.1-mm-thick high-silicon steel laminations and use continuous current mode (single pulse) operation above rated speed [20]. It seems that torque density and efficiency cannot be improved at the same time: for instance, [26] achieved an efficiency of 96% but torque density was 25 Nm/l, while [27] reported a torque density of 38 Nm/l, although the efficiency was 90% due to the low-grade iron steel utilized to maximize torque density. As usually in electrical machines, getting both high-torque density and high-energy efficiency is difficult without rare earth permanent magnets.

In SRDs, the power electronics topology is usually chosen as a compromise between performance and the number of power semiconductor devices. The higher the number of switches, the higher the cost and the failure rate, but the controllability of the system increases, improving performance. Different power topologies with specific advantages and disadvantages are usually found in the literature [1, 28, 29]. The most common one is the asymmetric bridge converter, comprising two switching devices and two power diodes per phase. **Figure 1** shows the circuit schematic of this converter for a 4-phase SRM. The main advantage of this topology is the capability of supplying each phase individually. This, in turn, allows efficient phase

overlapping, increasing average torque and reducing torque ripple. For the same reason, this circuit is very convenient for achieving fault-tolerant SRDs. In terms of cost, the main drawback of this topology is the high number of switching devices in comparison with other alternatives.

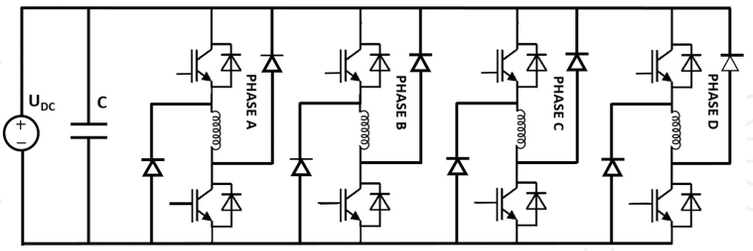

Figure 1. Asymmetric bridge converter topology for 8/6-pole switched reluctance machine.

The above topology requires two more diodes per phase compared with the most conventional topology used for PMSMs and IMs [30]. As aforementioned, some alternative topologies have been proposed in order to reduce the number of devices, including one that uses the SRM phases as inductive filters to charge the EV battery [31], which adds an additional value to this type of machine over IMs and PMSMs. However, these alternatives reduce the controllability and efficiency of the drive and are generally avoided in applications with demanding torque ripple requirements.

SRMs require very precise position determination, since the activation of the phases must be synchronized with rotor position to achieve good performance. Conventionally, SRDs have a measuring device (either an encoder or a resolver) to determine the speed and position of the rotor. These sensors are accurate and relatively inexpensive and have very good performance. However, it would be desirable to remove them (without deteriorating performance considerably) in order to make the drive cheaper, less voluminous, less noise-sensitive and more reliable [32, 33]. This can be done by means of a "position sensorless control", also known as "position self-sensing control" given that the external sensor is replaced by the electrical machine itself, which acts as its own position sensor [34].

As the cost and the volume of an external position sensor is not significant when compared to the whole traction system, the main advantage of position self-sensing in SRMs for EVs is the possibility to continue operation in case the external sensor is out of service. This redundancy increases the fault tolerance of the whole drive, which is critical in traction applications and one of the main approaches of this chapter.

During the last decades, many self-sensing techniques have been proposed for rotating electrical machines in general [32, 33] and SRMs in particular [35, 36]. Commonly, these methods perform well either at high speed (such as BEF-based, flux linkage-based or inductance-based techniques) or at low speed/standstill (such as injection-based or di/dt-based techniques). This implies that at least two of these methods are usually combined in the same drive, the transition between both being particularly delicate.

Besides, self-sensing normally causes a slight reduction in performance, since the position is estimated with some error. This in turn implies that phase activations and deactivations are not applied exactly when desired, leading to a reduction in average torque, an increase in torque ripple and its consequences, and a decrease in energy efficiency. Of course, all these disadvantages are minor when compared to having the possibility to operate the EV even after the external position sensor fails.

Electromagnetic interference (EMI) and electromagnetic compatibility (EMC) are also very important aspects of an EV. In this sense, SRMs could present worse EMC behavior due to higher di/dt and higher switching frequencies in general. Ample research is missing on this topic.

3. SRM under analysis: starting values for the design process

In this chapter, a SRM is analyzed from a preliminary point of view. For the sake of comparison, this SRM has been designed to replace the original PMSM of a Nissan Leaf, whose main specifications are listed in **Table 1**. Therefore, a SRM has to be pre-designed with the aim of achieving similar performance to that of the PMSM of the Nissan Leaf. This SRM must have the same torque-speed capabilities than the original motor. Besides, both machines should have the same outer diameter, while keeping current density at similar values, in an attempt to keep the comparison as fair as possible. As SRMs have significant lower power density than PMSMs, this means that the proposed SRM will be longer and heavier than the original motor.

Magnitude	Value (units)	Comments
Type of machine	PMSM	
Power (rated)	80 kW	
Torque (rated/max)	254/280 Nm	
Speed (rated/max)	3000/9800 rpm	Maximum speed estimated from vehicle parameters.
Transmission	7.94:1	Transformation ratio
DC voltage	300 V	Batteries rated voltage is 360 V, and batteries voltage ranges from 280 to 400 V depending on state of charge and current
Weight (PMSM)	82 kg	Estimated
Weight (inverter)	15 kg	Estimated
Stator outer diameter	250 mm	Estimated
Rotor outer diameter	170 mm	Estimated

Table 1. Nissan Leaf motor specifications.

The first decision to make when designing an electrical motor is obviously the machine type and topology (number of phases and number of poles). In this case, a conventional radial-flux inner-rotor non-skewed SRM is selected for consistency with the original PMSM. Regarding

the topology, an 8/6-pole configuration is chosen as a compromise between torque density + cost (the less number of phases/poles, the better) and torque ripple + degraded capability (the more phases/poles, the better) [2]. The minimum number of phases that can ensure that the machine will be able to start with m-1 phases available (degraded mode) from any rotor position is four (although a especial starting routine will sometimes be needed, which could also work for 3-phase SRMs; see Section 5). Hence, an 8/6-pole topology makes for a good candidate for fault tolerant EVs.

Input parameters		**Output parameters**	
Magnitude	**Symbol**	**Magnitude**	**Symbol**
Rated power	P_r	Number of turns per coil	N
Rated speed	ω_r	Phase current during activation; see **Figure 11a**	I_{AVG}
Number of stator phases	m	Rotor outer radius	R_R
Number of stator pairs per pole	N_{sp}	Active length	L
Stator outer radius	R_S	Stator pole width	$W_S = 2 \cdot a$
Air gap	g	Stator pole height	H_S
Operational current density	I_ρ		

Table 2. Input and output parameters for the analytical pre-design model.

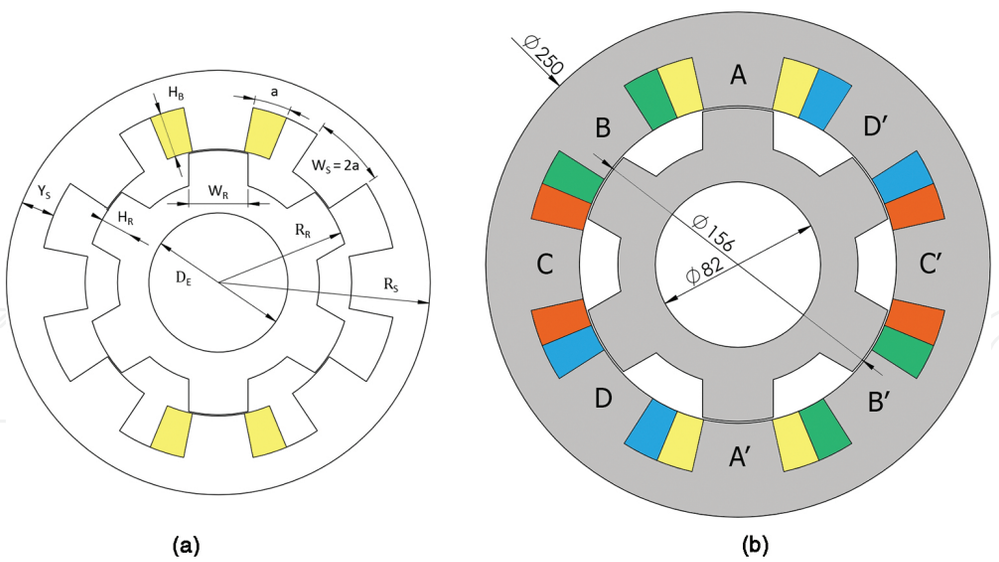

Figure 2. (a) Cross section of a 8/6-pole SRM with curved coils. (b) 80-kW SRM considered in this work (after FEM pre-design). Rotor position in both figures is 0° (phase AA′ aligned position).

Once the type of machine is fixed, the design process starts with analytical calculations based on some of the methodologies proposed in the literature, such as [35, 37, 38]. The main dimensions of a given SRM can be easily computed using a simple analytical model, which

starts from some initial specifications and several simplifications. Obviously, the results need to be checked with more refined tools such as finite element method (FEM) codes. Input parameters to perform the pre-dimensioning and output parameters to be provided by the model are given in **Table 2** and **Figure 2**.

Regarding the assumptions and simplifications in which the model is based, they can be listed as:

- The machine is fully saturated and works at a magnetic field B in the air gap, which leads to use a simple equation for the produced torque T, in the form:

$$T_{em} = \frac{P_r}{\omega_r} = 2 \cdot K_T \cdot N \cdot N_{sp} \cdot I_{AVG} \cdot B \cdot R_R \cdot L \tag{1}$$

  where K_T is a torque constant related to the machine saturation level, which varies from 0.5 in non-saturated machines up to 0.8 in heavily saturated ones. Additionally, the voltage V_k applied to each phase is:

$$V_k = 2 \cdot N \cdot N_{sp} \cdot \omega \cdot B \cdot R_R \cdot L \tag{2}$$

- Coils are curved for a better use of the slot between poles. They have the shape shown in **Figure 2**. Under this approach, it must be satisfied that:

$$N \cdot I_{AVG} = I_\rho \cdot a \cdot H_S \tag{3}$$

- The return yoke width Y_S must be the same as half the pole width in order to work at the same magnetic flux density at the return yoke, without increasing the saturation level. Alternatively, a certain correction empirical factor K_f can be introduced to achieve more realistic results. This simplification, together with some geometrical considerations, leads to the following expressions:

$$Y_S = K_f \cdot a \tag{4}$$

$$a = \frac{2 \cdot \pi \cdot R_R}{8 \cdot N_{sp} \cdot m} \tag{5}$$

$$R_S = R_R + H_S + Y_S \tag{6}$$

- Both coil ends can be considered as a complete circular ring with inner radius a and outer radius $2a$. This assumption allows an easy estimate of the overall length and weight of the coils.

Combining expressions (4)–(6), (3) and (1), one can derive an equation with two unknowns, the rotor radius R_R and the active length L :

$$R_S \cdot {R_R}^2 - {R_R}^3 \cdot \left(1 + \frac{\pi \cdot K_f}{4 \cdot N_{sp} \cdot m}\right) - \frac{T_{em} \cdot 2 \cdot m}{\pi \cdot K_T \cdot B \cdot L \cdot I_\rho} = 0 \xrightarrow{\text{fixing } L} -A \cdot {R_R}^3 + B \cdot {R_R}^2 - C = 0 \tag{7}$$

The procedure to dimension the machine consists in fixing the length L , and then finding the zeros of the polynomial function given by the above equation to calculate R_R. If the value chosen for L is too low, there will be no real solutions for the rotor radius R_R, meaning that for a given stator radius R_S there is no machine able to provide the required torque. Beyond that limit, there will be two main options: one with a small rotor radius and a large coil with many ampere-turns and another with a large rotor radius and a smaller coil. The optimum solution in terms of the shortest machine will be the one for which both rotor radiuses are the same. Alternatively, the criteria for finding the optimum machine could be to select the lightest one. In that case, the weight of the coil ends should be taken into account.

As an example, a pre-dimensioning of a SRM with the input specifications listed in **Table 3** has been performed.

Magnitude	Value (units)	Comments
Type of machine	8/6-pole SRM	m = 4, N_{sp} = 1
Power (rated)	80 kW	T_{em} = 254 Nm
Speed (rated)	3000 rpm	
Current density	7 A/mm^2	
Air gap magnetic field	1.8 T	
Pole to return Yoke factor	1	

Table 3. 8/6-pole SRM pre-design specifications.

Figure 3 shows the results obtained using the previous model, particularly the calculation of the optimum active length with its corresponding overall weight, for different stator outer radiuses. It can be seen that, for this simple approach, there is an optimum stator radius which minimizes the overall weight. Nevertheless, further and deeper analysis should be performed, since this solution can be far from being the optimum in terms of efficiency, for instance. In this regard, the evaluation of the coil resistance and inductance, end-winding included, is essential to estimate the behavior of the machine, including its overall efficiency.

http://dx.doi.org/10.5772/64431

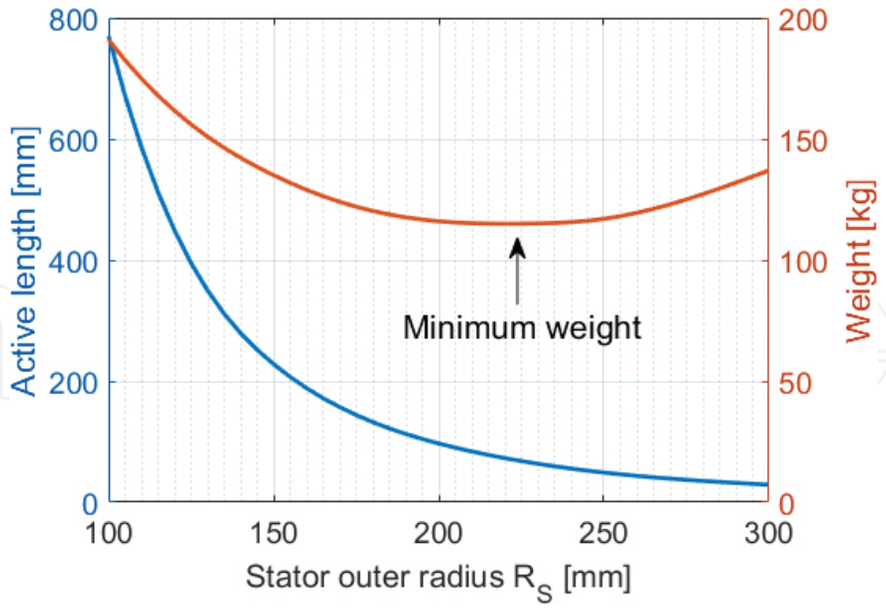

Figure 3. Calculation of active length and overall weight for the proposed SRM.

Magnitude	Minimum weight (analytical)	R_S = 125 mm, as the original PMSM (analytical)	R_S = 125 mm (FEM-tuned, Figure 2(b))
Active length **(mm)**	68	395	300
Stator radius **(mm)**	225	125	125
Rotor radius **(mm)**	124	72	78
Air gap	–	–	0.6
Stator pole width **(mm)**	49	28	34.3
Stator pole height **(mm)**	77	39	26.4
Turns per coil	29	8	10
Phase current I_{AVG} **(A)**	451	482	360
Current density (**A/mm²**)	7.0	7.0	7.7
Rotor pole width **(mm)**	–	–	35
Rotor pole height **(mm)**	–	–	18.5
Active weight **(kg)**	115 (est.)	156 (est.)	101

Table 4. Comparison between two possible analytical solutions for the proposed SRM and the tuned solution after the FEM simulations described in Section 4.

Table 4 provides the calculated output parameters for the minimum weight machine, along with those computed for a 250-mm outer stator diameter, which is the one designed to replace the original PMSM in the Nissan Leaf. **Table 4** also includes the parameters corresponding to the final pre-design, obtained after the design tuning achieved by FEM simulations and time-domain simulations such as those described in next section. This last design is the one that will be analyzed in detail for the rest of the chapter.

4. Pre-design analysis and validation

This section is devoted to the analysis and validation of the pre-design described in Section 3. This analysis was carried out only from an electrical engineering point of view, corresponding to an early-stage in the design process: electromagnetics, power electronics, modulation technique, control strategy and power losses. Therefore, other crucial aspects such as mechanical behavior, cooling, EMC, certification testing, series production, quality assurance, useful life and recyclability are not considered.

4.1. FEM analysis

The first step consists in analyzing and optimizing the preliminary design by means of FEM simulations. This task is usually divided into two different parts:

1. Verification of the analytical pre-design: The aim is to validate the topology, the main stator/rotor dimensions and the winding properties (e.g., number of turns) of the analytical pre-design. This means checking whether the machine provides rated torque at low speed with the specified current and current density, calculating the back-EMF (electromotive force) and the maximum speed for a given DC voltage, and other verifications such as air gap flux density, magnetic saturation or inductances.

2. Mild optimization of the geometrical design: FEM simulations are extremely useful to tune certain geometric parameters, such as stator and rotor pole widths and heights. This can be carried out in a very simple but suboptimal manner, or by considering an optimization problem which can be solved by conventional methods: from brute force (small number of design variables) to evolutionary algorithms.

For the purposes of this chapter, focus is placed on torque, both in normal and "m-1 phases" mode: average torque, torque ripple and minimum torque to start the vehicle (especially significant in degraded mode, when one of the phases is out of service). For such an analysis, 2D simulations are normally sufficient, especially for machines with a large ratio between magnetic length and rotor outer diameter ($L/D_R > 1$), which is the case analyzed here.

One of the first results that should be obtained by FEM simulations is the instantaneous torque as a function of both rotor position and current. It is sufficient to calculate it for half an electric period, since this function is periodical and asymmetrical with respect to the rotor angle. This period is calculated as follows:

$$\Delta\theta = \frac{360°}{N_R} \tag{8}$$

which yields 60° for an 8/6-pole SRM. Results for the 80-kW 8/6-pole SRM are depicted in **Figure 4**; rated current is 360 A. Notice how raising the current increases the saturation level

http://dx.doi.org/10.5772/64431

of the machine, which in turn "deforms" the torque pulse. This deformation implies higher torque ripple under constant current profiles, as described later.

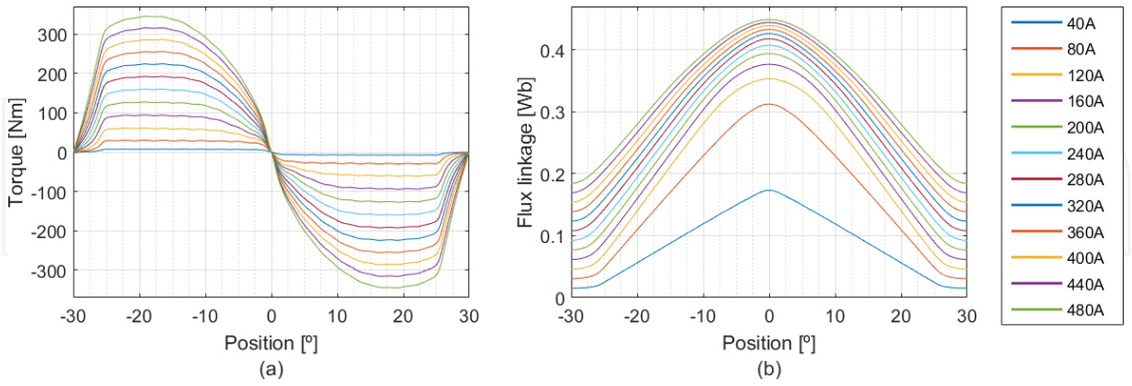

Figure 4. (a) Instantaneous torque and (b) flux linkage during an electric period for different current values.

It is also very interesting to calculate the flux linkage of each phase as a function of rotor position and current, as shown in **Figure 4**. This information is extremely useful to build a simulation model of the whole traction drive, as described in Section 4.3. Notice that most SRM models found in the literature neglect cross-coupling between phases, which implies that each phase is supposed to be independent of the rest. This assumption is not valid under operating conditions in which two phases conduct simultaneously. This is especially relevant when torque is generated by two phases (such as phase overlapping in torque-sharing functions to reduce torque ripple).

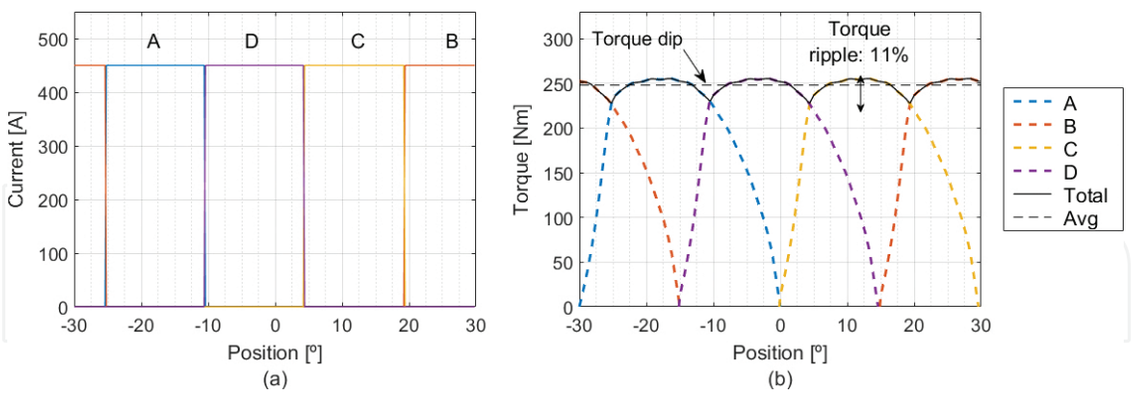

Figure 5. (a) Ideal current pulses and (b) corresponding torque profile at 100% load.

Next, torque curves from **Figure 4** can be post-processed to estimate the instantaneous torque profile in steady state for different current levels. Usually, this is carried out under the assumption of ideal current pulses, such as those depicted in **Figure 5**. Of course, this ideal supply is far from being real, but it gives a first estimation without using a full model of the drive, such as the one described later in the chapter. In this ideal case, the activation and deactivation angles θ_{ON} and θ_{OFF} are given by the intersection of the torque curves corre-

sponding to different phases, so that there is no overlapping (the previous phase is turned off when the next one is turned on). The torque profile corresponding to these ideal current profiles is shown in **Figure 5** for rated current. Notice how a constant current profile without overlapping cannot generate a constant torque profile in non-skewed SRMs, even at low current levels (low saturation levels).

Finally, FEM results can also be used to assess the degraded capability of an SRM. **Figure 6** shows the current profile under ideal current pulses when one of the phases is out of service. Compared to normal operation (**Figure 5**), m-1 mode presents lower torque and extremely high-torque ripple under ideal current pulses supply. It is worth mentioning that switching angles should be specifically optimized for degraded operation, so that the control strategy can adapt to the new topology when a phase losses its function. Therefore, the average torque and torque ripple values included in **Figure 6** are not final, as presented later in this chapter.

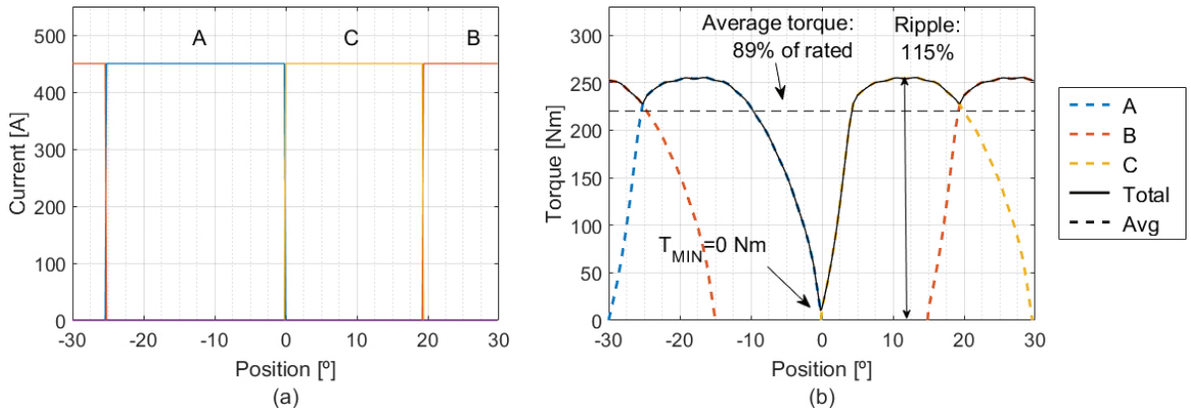

Figure 6. Torque profile in degraded mode of operation (m-1 phases).

Speed (rpm)	Mode	Conduction losses (W)	Switching losses (W)	Total losses (W)	Efficiency (%)
3000	Normal	2254	1161	3415	96.8
9800	Normal	2102	305	2407	97
3000	m-1 phases	1256	771	2050	97.43
9800	m-1 phases	912	368	1280	98.4

Table 5. Power electronics losses in steady state at rated and maximum speed, both for normal and degraded modes.

Similarly, it is convenient that the torque dip generated by the missing phase is above 0 at every angle to ensure that the vehicle can start regardless of rotor position (this is not possible with 6/4-pole and 8/6-pole SRMs). Otherwise, special starting routines must be implemented in the control system, as proposed in **Table 5**. There are many factors that influence the capability of a given SRM to start an EV besides rotor position: inertia, load torque (including the grade of the road α), overloading capability of the traction drive and the control strategy, which can be adapted to the particular conditions in which the vehicle must be

started. Further analysis regarding the self-starting capability under degraded operation is presented in section 5.

4.2. Power electronics pre-design

Power electronics to drive the 8/6-pole SRM comprises an asymmetric power converter connecting to the common DC link for all electric phases and a DC filter to improve voltage ripple. The electrical machine is current-controlled by means of a hysteresis band strategy. Other usual alternatives are closed-loop pulse-width-modulation (PWM) [39] and direct torque control (DTC) [40].

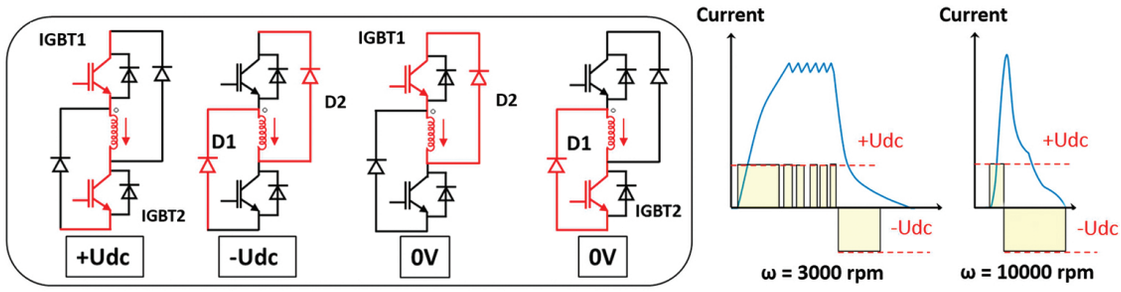

Figure 7. SRM power converter topology and switched selection for rated and maximum speed operation.

Motor mode operation requires the use of $+U_{DC}$ and 0 V to keep the current within the reference band, using $-U_{DC}$ to switch the current off rapidly when the phase is deactivated, as **Figure 7** illustrates. Current is individually controlled in each machine phase with an asymmetric bridge topology, allowing total independence between phases. During EV braking, the machine works as a generator, requiring $+U_{DC}$ to increase rapidly the current and then it is kept within the reference band using 0 V and $-U_{DC}$. At higher speeds, the machine is designed to achieve single-pulse operation, where just $+U_{DC}$ and $-U_{DC}$ are sufficient to control the current whilst the commutation frequency is reduced [41].

Since the power level and the DC-link voltage are usually defined, simulation-based analysis can be used to determine the voltage and current levels of the power converter devices. The semiconductor technology is selected to fulfill the following electrical specifications: DC-link voltage, current carrying capacity, maximum switching frequency, load cycle and isolation requirements.

4.3. Drive modeling and analysis

When analyzing electrical drives, simulation models in the time-domain comprising the electrical machine, the power electronics converter, the control strategy, the switching technique and the equivalent load are extremely useful. When the machine model is built with data extracted from FEM simulations (employing tools such as look-up tables or LUTs), these kind of simulations allow for fast and accurate calculations. In the case of SRDs, such a model is an excellent way to calculate average torque and torque ripple under real current pulses and

also to optimize switching angles under different operating conditions and optimization criteria. **Figure 8** shows a schematic of the time-domain simulation model used in this work.

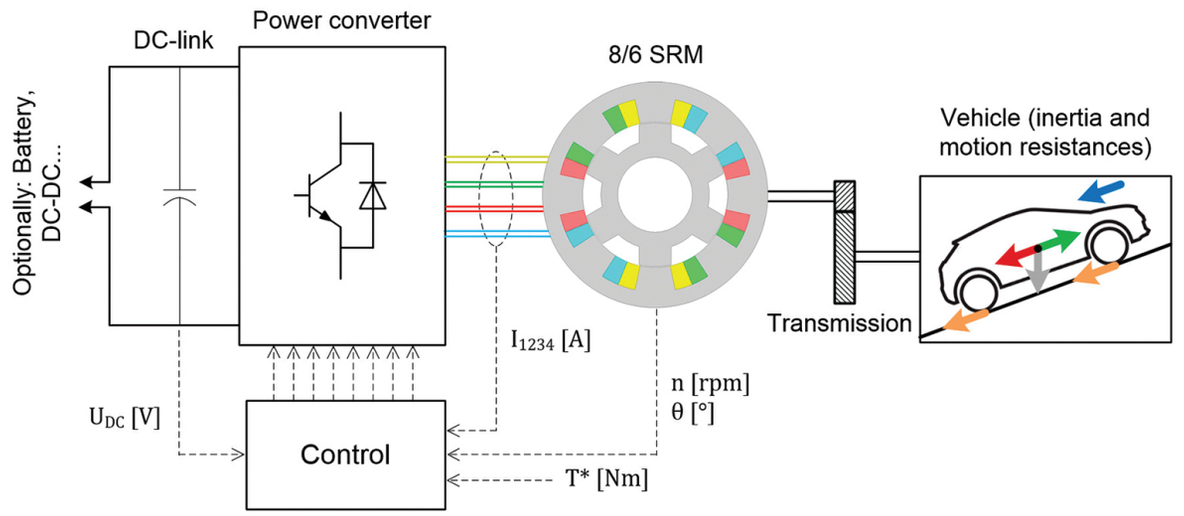

Figure 8. SRM-based traction drive model.

SRDs and EVs modeling is outside the scope of this chapter, and therefore, the reader is referred to publications that deal with these aspects, such as [1, 42–45]. For convenience, the most relevant equations are included next, starting with the voltage equation for each machine phase:

$$u_k = R_S \cdot i_k + \frac{d\lambda_k}{dt}; \quad k = 1 \ldots m \tag{9}$$

The flux linkage λ_x of each phase depends on the current of that phase i_x, of the current of the previous/next phase i_y (when simultaneous conduction takes place) and rotor position θ. Neglecting cross-coupling yields:

$$\lambda_k = f(i_k, i_{k\pm1}, \theta) \approx f\left(i_k, \theta\right) \tag{10}$$

the relationship between flux linkage, current and rotor position being the one given by **Figure 4**, usually implemented via a LUT. Similarly, the torque provided by each phase is given by **Figure 4** and a second LUT, the total torque being the sum of each phase torque (again, cross-coupling is neglected):

$$T_{em} = T_k + T_{k+1}; \qquad T_k \approx g\left(i_k, \theta\right) \quad \text{and} \quad T_{k+1} \approx g(i_{k+1}, \theta) \tag{11}$$

Notice that the above expression considers up to two phases because it will be the maximum number of phases conducting simultaneously. Finally, the mechanical equation of the drive is as follows:

$$T_{em} - T_{load} = J \cdot \frac{d\omega_{mec}}{dt} + B \cdot \omega_{mec} \tag{12}$$

The vehicle model represents both the total inertia and the load torque as seen by the motor:

$$J \approx J_{rotor} + \frac{J_{wheels}}{i_{GEAR}^{\ 2}} + \frac{M \cdot ERR^2}{i_{GEAR}^{\ 2}} \tag{13}$$

$$T_{load} = \frac{ERR}{i_{GEAR} \cdot \mu_{GEAR}} \cdot F_T \ (traction\ mode) \tag{14}$$

where M is the total mass of the vehicle [kg], ERR [m] is the effective rolling radius, i_{GEAR} [−] is the transmission gear ratio and μ_{GEAR} [−] is the transmission energy efficiency (assumed to be constant and equal to 0.95).

The vehicle motion resistances include rolling resistance, aerodynamic drag and gradient resistance; the last one being of active nature (may take negative values and contribute to the movement of the vehicle):

$$F_T = F_{aero} + F_{roll} + F_{grav} \rightarrow \begin{cases} F_{aero} = \frac{1}{2} \cdot \rho \cdot A_F \cdot C_D \cdot v^2 \geq 0 \\ F_{roll} = \mu_{rod} \cdot M \cdot g \cdot \cos(\alpha) > 0 \\ F_{grav} = M \cdot g \cdot \sin(\alpha) \end{cases} \tag{15}$$

Regarding the control strategy and the switching technique, this work considers hysteresis current control with optimized switching angles as a function of speed and the desired torque, as illustrated in **Figure 9**.

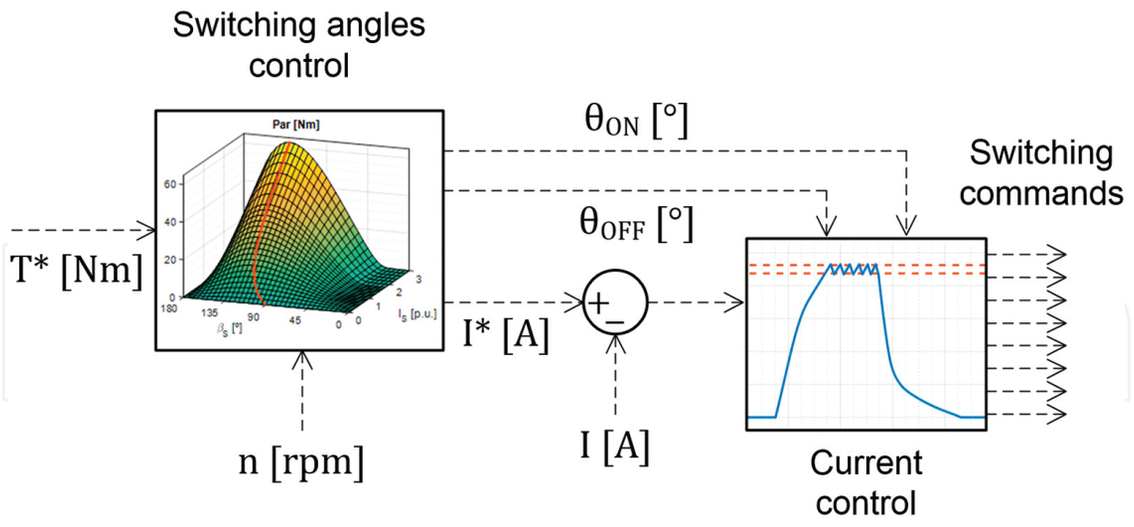

Figure 9. Torque control scheme with switching angles controller.

A simulation model such as the one described above is useful to optimize switching angles considering different optimization criteria. In this particular case, a compromise between average torque and torque ripple was chosen, which yields the torque-speed characteristic depicted in **Figure 10** (angle resolution of ±0.25°).

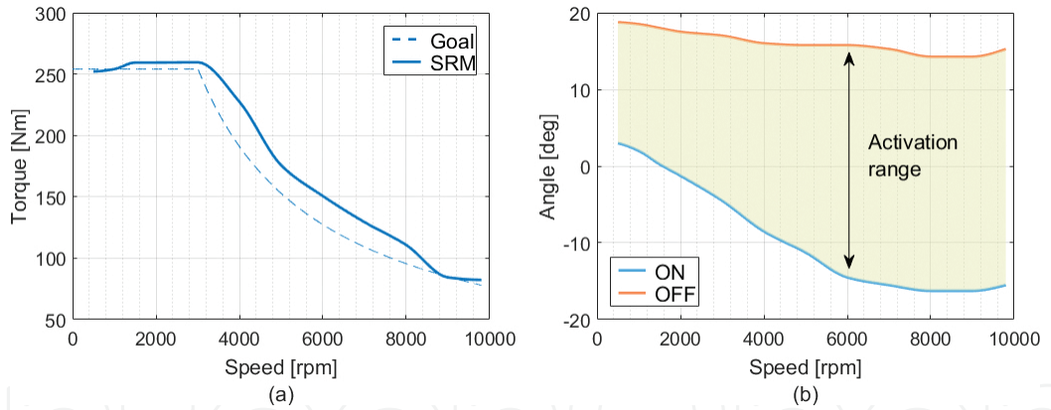

Figure 10. (a) Torque-speed characteristic of the 8/6-pole SRM analyzed in this chapter. (b) Corresponding switching angles as a function of speed (all phases are equal but phase-shifted).

Traditionally, one of the biggest disadvantages of SRMs is torque ripple and its consequences (vibrations, efficiency and acoustic noise) with respect to other electrical machines. However, there has been a lot of research on this topic in the last two decades. As a result, torque ripple has improved considerably and it is no longer an issue in many applications that use SRMs. Basically, there are two main approaches to reduce torque ripple (which can be complementary): machine design and machine control. The former include techniques such as skewing (see Section 2 for references). These modifications reduce overall performance (torque density and efficiency) and could increase the cost of the machine.

http://dx.doi.org/10.5772/64431

The second alternative consists in improving the control strategy. These methods can be classified into two categories, depending on whether the converter topology is conventional or advanced [44]. Examples of control strategies belonging to the first category are current profiling or current shaping (CP), torque-sharing function (TSF) and direct torque control (DTC). The first two basically consist in adapting the shape of the real current pulses so that torque dips/peaks are minimized [35]. Of course, this adaptation will be feasible depending on the available voltage, the back-EMF of the machine, and the inductance. In other words, the feasibility will decrease with the speed of the machine. This is convenient, given that torque ripple is more detrimental at low speed, both mechanically and from the point of view of comfort. Advanced topologies use a second DC source to increase the available voltage under certain operating conditions, thus allowing for higher *di*/*dt* [44].

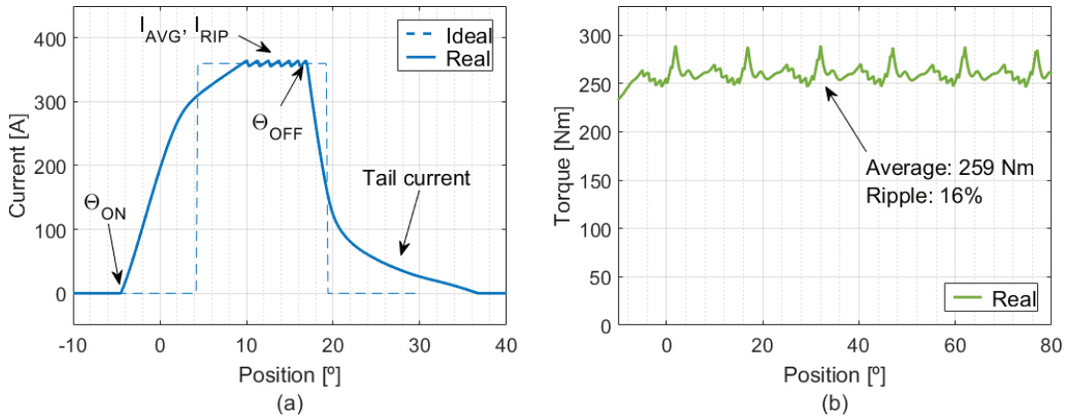

Figure 11. (a) Current pulse considered in this work (no current profiling) and (b) corresponding torque profile, both at 3000 rpm and 100% load.

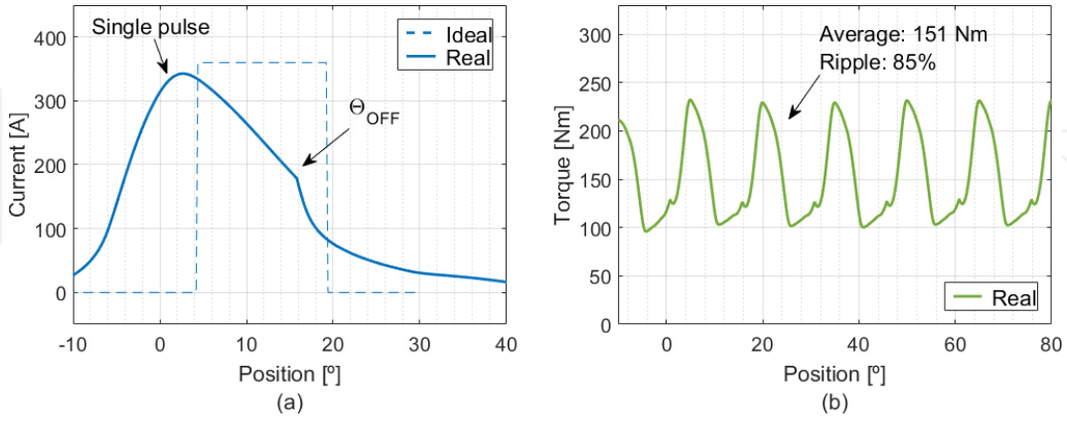

Figure 12. (a) Current in single pulse mode and (b) corresponding torque profile, both at 6000 rpm and 100% load.

For the sake of simplicity, and unless otherwise stated, all the results presented are given for a current control scheme which operates with unshaped current pulses such as that depicted in **Figure 11**, defined by θ_{ON}, θ_{OFF}, I_{AVG} and I_{RIP}. Consequently, torque ripple values given in

this chapter are noticeably high and should not be considered as reference values for EV applications.

Finally, **Figure 12** contains the same information as **Figure 11** but for a high-speed operating point. As speed increases, the time available for each phase activation reduces and at the same time the phase back-EMF increases, which makes the machine work in single pulse mode (also known as advance angle control or AAC by some authors, although this name could be confusing because turn-on angles are advanced in a wide range of speed, and not only under single pulse operation).

4.4. Power losses analysis

Power losses in SRDs present some differences when compared to those based in IMs or PMSMs. When a machine works with sinusoidal current supply, simplified loss models based on single-frequency models of the machine are usually sufficient to estimate resistive losses in the electrical circuit and iron losses in the magnetic circuit. However, SRMs have pulsed supply, which invalidates the single-frequency approach.

Resistive losses (also known as Joule or copper losses) depend on three main factors: the current i, the DC resistance of the winding R_{DC} (defined by its cross-sectional area, its total length and its conductivity) and the skin effect and proximity effect factor k_{AC} (which gives the AC resistance of the winding and depends on its geometrical properties and the frequency of the current) [37]. Therefore, the instantaneous power dissipated in each coil is:

$$P_{Cu,1}(t) = f\left(i, R_{DC}, k_{AC}\right) = k_{AC} \cdot R_{DC} \cdot i(t)^2 = R_{AC} \cdot i(t)^2 \tag{16}$$

In steady state, average power losses may be estimated analytically using the RMS value of the current and the total number of phases m:

$$\overline{P_{Cu}} = m \cdot R_{AC} \cdot {I_{RMS}}^2 \approx m \cdot R_{AC} \cdot \left(\frac{I_{AVG}}{\sqrt{m}}\right)^2 = R_{AC} \cdot {I_{AVG}}^2 \tag{17}$$

In practice, resistive losses will be higher to those estimated by the above equation, since it assumes ideal current pulses and therefore neglects current tails and phase overlapping. A simulation model such as that described in Section 4.3 can prove accurate to estimate resistive losses with real current profiles, provided that the skin and proximity effects factor k_{AC} has been properly considered. Notice that such factor depends on the switching frequency, and hence an iterative process may be required. For the SRM analyzed in this work, $k_{AC} \approx 3$.

Both skin and proximity effects are caused by eddy currents in the windings of the machine. High-power low-voltage SRMs such as those used for EV applications are usually strongly affected by these phenomena due to the combination of low number of turns, large cross-sectional area in the conductors and currents with high-frequency components in the frequen-

cy domain. As the wire dimensions increase, eddy currents gain importance and neglecting them can lead to significant overestimation of machine performance [46]. As it is well-known, methods such as conductor division and transposition, employing parallel paths or using Roebel bars or Litz wire, help reduce k_{AC}.

Iron losses are also very relevant in high-speed rotating machines. They depend on the magnetic flux density amplitude and frequency, and thus on the machine current and speed:

$$P_{Fe} = f_1(B, f) = f_2(I_{AVG}, n) \tag{18}$$

Again, conventional iron loss estimation techniques based on single-frequency models are not suitable for SRMs, whose current is pulsated and not sinusoidal [47]. In general, SRMs have higher frequencies and higher harmonic content than other machines at comparable speed and power, but less iron volume in high-speed applications [48]. Another distinctive aspect of SRMs is that some iron regions work with bidirectional magnetic flux, while in others the flux is unidirectional. In this sense, the number of flux reversals in the rotor can be minimized using negative current pulses. Hence, designing a SRD with bidirectional current supply can greatly improve rotor iron losses, at the expense of doubling the number of power switches.

Mechanical losses comprise bearing losses, windage losses and air-cooling losses when forced convection is used. Bearing and air-cooling losses in SRMs are comparable to other machines types and they are modeled in the same way. Windage losses, however, are usually higher in SRMs due to their doubly salient nature, and more specifically, to the aerodynamic behavior of the salient pole rotor. This is usually an issue in high-tangential speed applications, in which vacuum chambers or vacuum sleeves are sometimes used for this reason. Windage losses calculations that assume cylindrical rotor shape are not valid for conventional SRMs and hence specific expressions must be used:

$$P_{wind} = A \cdot \omega^B; B \in [2,3] \tag{19}$$

where A and $B \in [2, 3]$ are coefficients which depend on the rotor geometry, and in the case of A also on the operating conditions (pressure, temperature, etc.) [49].

Power electronics losses are also very relevant in electrical drives. They are usually divided into static and switching losses. The former refer to steady state (on- and off-states) while the latter refers to transients between states (switching). Conduction losses are of the first kind, as they correspond to the nonzero on-state voltage of the device V_{ON} (collector-emitter voltage in an IGBT (Isolated Gate Bipolar Transistor), emitter-collector voltage in a diode) while it carries a current I_{ON} [50]. The other static losses are those corresponding to the nonzero off-state current of a power semiconductor device when it blocks a voltage V_{OFF}. This reverse current I_{OFF} is a leakage current which in turn depends on V_{OFF} and which is usually very low for the power levels considered in this work. Therefore, blocking losses are conventionally

neglected in IGBTs except for high voltages (above 1000 V) and/or high temperatures (above 150°C) [50, 51].

$$P_{COND} = P_{ON} + P_{OFF} \approx P_{ON} = f(V_{ON}, I_{ON}, Temp.) \tag{20}$$

Complementary, the energy dissipated during each switching is called either turn-on energy E_{ON} or turn-off energy E_{OFF}. Neglecting parasitic effects, switching losses are given by the following expression [52]:

$$P_{SW} = P_{SW,ON} + P_{SW,OFF} = \left(E_{ON} + E_{OFF}\right) \cdot f_{SW} \tag{21}$$

f_{SW} being the switching frequency. Obviously, both E_{ON} and E_{OFF} highly depend on the current and on the voltage, since they are defined by a power peak that in turn is caused by current and voltage transients. They are also influenced by temperature. The switching frequency measures the number of turn-ons and turn-offs per time unit of a power semiconductor. It depends on the operating point (torque and speed) and on the electrical characteristic of the machine. In a 8/6-pole SRM, each phase is enabled six times per rotor revolution, so that knowing speed in the machine (e.g., 3000 rpm) and the number of commutations per phase activation n_C, the switching frequency is given as:

$$f_{sw,avg}(Hz) = \frac{3000 \text{ rpm}}{1 \text{ min}} \cdot \frac{1 \text{ min}}{60 \text{ s}} \cdot \frac{6 \text{ activation}}{1 \text{ revolution}} \cdot \frac{n_C}{\text{activation}} = 300 \cdot n_C \tag{22}$$

In single pulse mode, n_C is reduced to only two commutations per phase activation. As a result, switching losses decrease significantly.

For the sake of illustration, total power losses have been calculated for the SRD studied in this work under rated electrical conditions (U_{DC} = 300 V, I_{AVG} = 360 A and n = 3000 rpm) and maximum speed (n_{nom} = 9800) using simulation analysis. Besides, power losses have been calculated in degraded mode of operation (m-1 phases available) as well. **Table 5** shows the results for both modes of operation (normal and degraded).

5. Degraded mode (with m-1 phases available)

As mentioned along the whole chapter, "m-1 phases" operation is particularly interesting in EV applications and one potential advantage of SRMs over its counterparts. Degraded mode was one of the main reasons why a 4-phase topology was chosen in this work, given that

performance loss, when one phase losses functionality, is obviously more significant in machines with a low number of phases.

Performance priorities under these circumstances are different from those in normal operation. Degrade mode will be used only in case of emergency: it will allow the EV to keep driving, but the owner should take it to a repair workshop as soon as possible for proper fixing (similar to an emergency spare tire). This consideration has many implications. For instance, switching angles optimization should probably prioritize average torque over torque ripple, which will be huge anyway, or even over energy efficiency or IGBT (Isolated Gate Bipolar Transistor) aging.

Degraded mode is implemented by detecting that one phase cannot operate anymore (severe fault detection), by disabling it, and by adapting the control strategy to the new situation so that performance loss is minimized. Fault detection may be carried out in different ways, such as [53–55]. Faults that can be surpassed by the aforementioned m-1 phases mode include single coil faults, single IGBT faults and single converter branch faults, which are the most frequent. Notice that those faults that affect more than one phase simultaneously will generally prevent operation in degraded mode, unless the number of phases is high (five or more). In any case, grave faults such as DC-link short circuits will completely prevent operation.

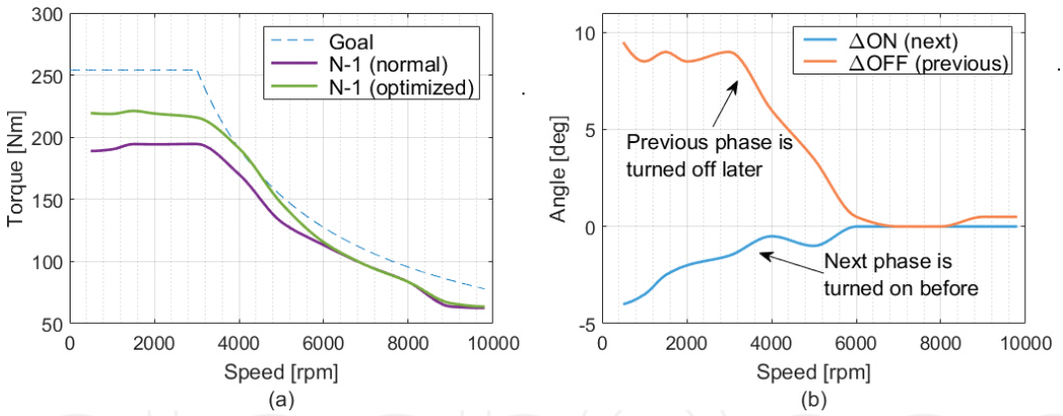

Figure 13. (a) Torque-speed characteristic of the 8/6-pole SRM in m-1 phases mode. (b) Modification of switching angles with respect to the normal mode.

Performance analysis under degraded mode can be carried out with the same methodology presented in Section 4.3. For instance, **Figure 13** shows the torque-speed characteristic of the 8/6-pole SRM in m-1 phases mode. Two curves are given: one corresponding to default switching angles (those used in normal mode) and a second obtained by optimizing the angles specifically for m-1 phases operation, thus increasing torque but also current loading in both the power converter and the machine. In this last case, one of the phases is disabled, and consequently the adjacent phases are used in a wider range of angular position, as depicted in **Figure 6** for an ideal case. Namely, the previous phase is turned off later than usual, while the next phase is activated before, as shown in **Figure 13**.

Complementary, **Figure 14** shows the current pulses in steady state in "m-1 phases" mode. The torque profile is also depicted. It is worth mentioning that increasing the conduction period of the adjacent phases implies overloading both the corresponding power electronics and some of the machine coils from the thermal point of view. Therefore, results from **Figures 13** and **14** could be invalid for long periods of operation (in this sense, angles corresponding to normal mode are a safer choice). However, in this work, current was kept constant for the sake of comparison.

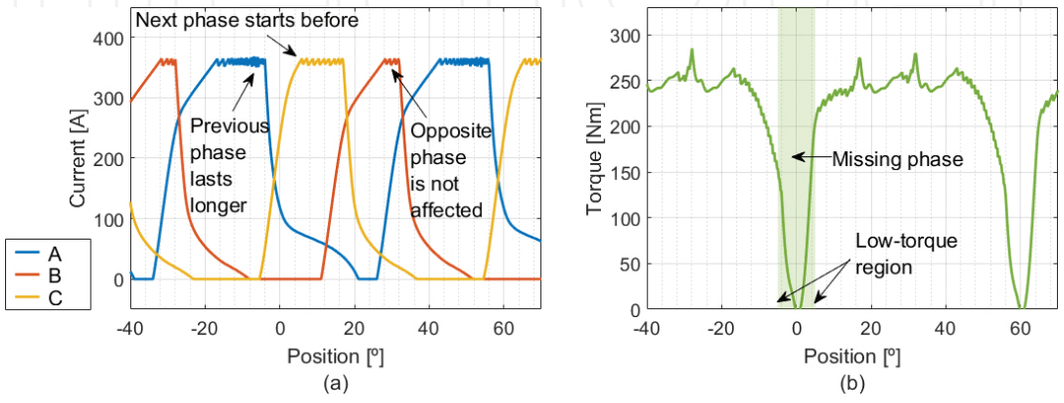

Figure 14. (a) Current pulses in m-1 phases mode (phase D is disabled) and (b) corresponding torque profile, both at 3000 rpm and 100% current.

It is important to notice that degraded mode should be able not only to keep the EV running, but also to start it from any rotor position and from different conditions, such as different road grade values. In this sense, when rotor position implies that a rotor pole is aligned with phase A in **Figure 2** (i.e., $\theta = 0° \pm k \cdot 60°$; see **Figure 6**), there is no available torque. In practice, torque is very low in a zone of $\pm 5°$ around these zero-torque positions (see **Figure 14**), which constitute the worst situation to start the vehicle. There are at least three possible ways to proceed in such a case, depending on the road grade:

- Negative grade (gravitational force helps starting the vehicle): this is the best case, since it is sufficient to release the mechanical brakes and let the vehicle start going down the slope. After 10 mechanical degrees in the motor shaft, which imply barely 7 mm of linear displacement in this particular case, the motor can already provide enough torque to further accelerate the vehicle at reasonable rates.

- Positive grade (gravitational force opposes vehicle movement in the desired direction): this is the case which requires more torque and therefore the one in which the torque reduction, due to the faulty phase, will be more noticeable during acceleration. However, starting the vehicle is not so difficult, provided that it can move backwards for at least 7 mm. The starting process would comprise two steps: First, mechanical brakes are released and the vehicle reverses, down the slope, until the motor gets out of the low-torque zone, and then it is stopped. Second, high torque is provided by the motor to start the vehicle again, knowing that a torque dip will appear almost as soon as the vehicle starts moving. However, if the

speed of the vehicle is not enough to go through the whole low-torque region, the vehicle will stop due to the gravitational force. This would require repeating the process, but making the linear displacement in step 1 larger, so that higher speed can be achieved before facing the low-torque zone.

- Flat road (there is no gravitational force): the main problem here is that releasing the mechanical brakes will not start the vehicle. However, a two-step starting process similar to that described above could suffice: First, the phase opposite to the faulty one (if the activation sequence is A–B–C–D and D is the faulty phase, then B is the phase opposite to the faulty one), which has high negative torque capability precisely when the rotor is in the low-torque region, is used to reverse the vehicle for up to 7 mm. For this, it is very convenient that the SRM has an even number of phases, so that the phase opposite to the faulty one can provide high torque (although more than one phase can be used otherwise, as usually in SRMs). The second step is exactly the same as in the case of positive grade, but without the gravitational force opposing acceleration, which highly simplifies the starting process.

As an example, a starting process such as that described above is shown in **Figure 15**, corresponding to a flat road situation. As can be seen, the results suggest that the proposed starting protocol would successfully start a Nissan Leaf with the 8/6-pole SRM studied in this work.

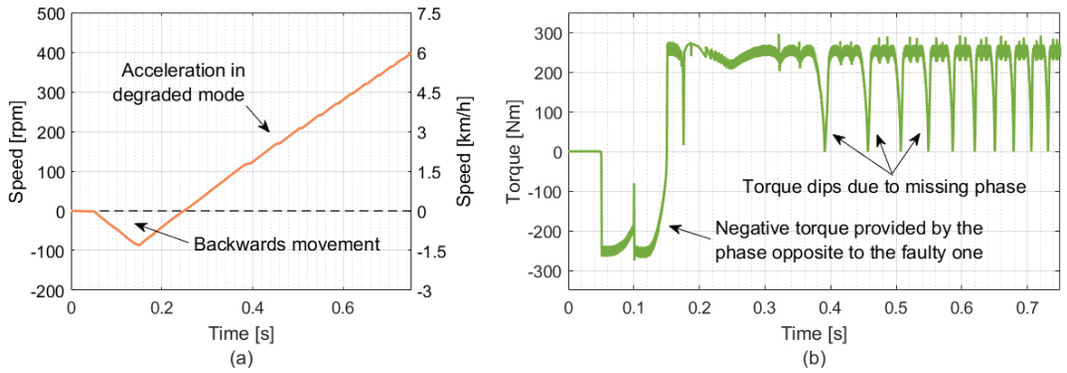

Figure 15. Vehicle start-up from the worst possible rotor position (none of the healthy phases produce torque) and under the worst possible conditions (flat terrain).

Author details

Pablo Moreno-Torres*, Marcos Lafoz*, Marcos Blanco, Gustavo Navarro, Jorge Torres and Luis García-Tabarés

*Address all correspondence to: pablo.moreno-torres@ciemat.es and marcos.lafoz@ciemat.es

Electrical Engineering Department, CIEMAT (Spanish National Research Centre on Energy, Environment and Technology), Madrid, Spain

References

[1] Krishnan R. Switched Reluctance Motor Drives: Modeling, Simulation, Analysis, Design, and Applications. 1st ed: CRC Press LLC Boca Raton, Florida, United States ; 2001.

[2] Petrus V, Pop AC, Martis CS, Gyselinck J, Iancu V, editors. Design and comparison of different Switched Reluctance Machine topologies for electric vehicle propulsion. In: 2010 XIX International Conference on Electrical Machines (ICEM); 2010 6–8 Sep. 2010.

[3] Takeno M, Chiba A, Hoshi N, Ogasawara S, Takemoto M, Rahman MA. Test Results and torque improvement of the 50-kW switched reluctance motor designed for hybrid electric vehicles. IEEE Transactions on Industry Applications. 2012;48(4):1327–34.

[4] Staunton RH, Ayers CW, Marlino LD, Chiasson JN, Burress TA. Evaluation of 2004 Toyota Prius Hybrid Electric Drive System. R. H. Staunton C. W. Ayers L. D. Marlino J. N. Chiasson T. A. Burress Prepared by the OAK RIDGE NATIONAL LABORATORY Oak Ridge, Tennessee 37831 managed by UT-BATTELLE, LLC for the U.S. DEPARTMENT OF ENERGY Under contract DE-AC05-00OR22725 Publication Date: May 2006 http://www.engr.uvic.ca/~mech459/Pub_References/890029.pdf

[5] Kiyota K, Sugimoto H, Chiba A. Comparing electric motors: an analysis using four standard driving schedules. IEEE Industry Applications Magazine. 2014;20(4):12–20.

[6] Anekunu AY, Chowdhury SP, Chowdhury S, editors. A review of research and development on switched reluctance motor for electric vehicles. In: 2013 IEEE Power and Energy Society General Meeting (PES); 2013 21–25 July 2013.

[7] Cheng H, Chen H, Yang Z. Average torque control of switched reluctance machine drives for electric vehicles. IET Electric Power Applications. 2015;9(7):459–68.

[8] Jack AG, Mecrow BC, Haylock JA. A comparative study of permanent magnet and switched reluctance motors for high-performance fault-tolerant applications. IEEE Transactions on Industry Applications. 1996;32(4):889–95.

[9] Stephens CM. Fault detection and management system for fault-tolerant switched reluctance motor drives. IEEE Transactions on Industry Applications. 1991;27(6):1098–102.

[10] Mir S, Islam MS, Sebastian T, Husain I. Fault-tolerant switched reluctance motor drive using adaptive fuzzy logic controller. IEEE Transactions on Power Electronics. 2004;19(2):289–95.

[11] Hennen MD, Niessen M, Heyers C, Brauer HJ, Doncker RWD. Development and control of an integrated and distributed inverter for a fault tolerant five-phase switched reluctance traction drive. IEEE Transactions on Power Electronics. 2012;27(2):547–54.

[12] Zeraoulia M, Benbouzid MEH, Diallo D. Electric motor drive selection issues for HEV propulsion systems: a comparative study. IEEE Transactions on Vehicular Technology. 2006;55(6):1756–64.

[13] Sebastian T. Temperature effects on torque production and efficiency of PM motors using NdFeB magnets. IEEE Transactions on Industry Applications. 1995;31(2):353–57.

[14] Desai PC, Krishnamurthy M, Schofield N, Emadi A. Novel switched reluctance machine configuration with higher number of rotor poles than stator poles: concept to implementation. IEEE Transactions on Industrial Electronics. 2010;57(2):649–59.

[15] Bilgin B, Emadi A, Krishnamurthy M. Design considerations for switched reluctance machines with a higher number of rotor poles. IEEE Transactions on Industrial Electronics. 2012;59(10):3745–56.

[16] Rallabandi V, Fernandes BG. Design procedure of segmented rotor switched reluctance motor for direct drive applications. IET Electric Power Applications. 2014;8(3):77–88.

[17] Moallem M, Ong CM, Unnewehr LE. Effect of rotor profiles on the torque of a switched-reluctance motor. IEEE Transactions on Industry Applications. 1992;28(2):364–69.

[18] Krzysztof Bieńkowski JS, Bogdan Bucki, Adam Biernat, Adam Rogalski. Influence of Geometrical Parameters of Switched Reluctance Motor on Electromagnetic Torque. Berichte Und Informationen Hochschule fur Technik und Wirtschaft; Dresten 2004.

[19] Sundaram M, Navaneethan P, Vasanthakumar M, editors. Magnetic analysis and comparison of Switched Reluctance Motors with different stator pole shapes using a 3D finite element method. In: 2009 INCACEC 2009 2009 International Conference on Control, Automation, Communication and Energy Conservation; 2009 4–6 June 2009.

[20] Chiba A, Kiyota K, Hoshi N, Takemoto M, Ogasawara S. Development of a rare-earth-free SR motor with high torque density for hybrid vehicles. IEEE Transactions on Energy Conversion. 2015;30(1):175–82.

[21] Uematsu T, Wallace RS, editors. Design of a 100 kW switched reluctance motor for electric vehicle propulsion. In: 1995 APEC '95 Conference Proceedings of Applied Power Electronics Conference and Exposition;1995, Tenth Annual; 1995 5–9 Mar 1995.

[22] Rahman KM, Schulz SE. Design of high-efficiency and high-torque-density switched reluctance motor for vehicle propulsion. IEEE Transactions on Industry Applications. 2002;38(6):1500–07.

[23] Watanabe K, Aida S, Komatsuzaki A, Miki I, editors. Driving force characteristics of 40 kW switched reluctance motor for electric vehicle. In: 2007 ICEMS International Conference on Electrical Machines and Systems; 2007 8–11 Oct. 2007.

[24] Shuanghong W, Qionghua Z, Zhiyuan M, Libing Z. Implementation of a 50-kW four-phase switched reluctance motor drive system for hybrid electric vehicle. IEEE Transactions on Magnetics. 2005;41(1):501–04.

[25] Kalan BA, Lovatt HC, Prout G, editors. Voltage control of switched reluctance machines for hybrid electric vehicles. Power Electronics Specialists Conference, 2002 pesc 02 2002 IEEE 33rd Annual; 2002 2002.

[26] Watterson PA, Wei W, Kalan BA, Lovatt HC, Prout G, Dunlop JB, et al., editors. A switched-reluctance motor/generator for mild hybrid vehicles. In: 2008 ICEMS 2008 International Conference on Electrical Machines and Systems; 2008 17–20 Oct. 2008.

[27] Miller JM, Gale AR, McCleer PJ, Leonardi F, Lang JH, editors. Starter-alternator for hybrid electric vehicle: comparison of induction and variable reluctance machines and drives. Industry Applications Conference, 1998 Thirty-Third IAS Annual Meeting The 1998 IEEE; 1998 12–15 Oct. 1998.

[28] Ellabban O, Abu-Rub H, editors. Switched reluctance motor converter topologies: a review. In: 2014 IEEE International Conference on Industrial Technology (ICIT); 2014 Feb. 26 2014-March 1 2014.

[29] Barnes M, Pollock C. Power electronic converters for switched reluctance drives. IEEE Transactions on Power Electronics. 1998;13(6):1100–11.

[30] Miller TJE. Converter volt-ampere requirements of the switched reluctance motor drive. IEEE Transactions on Industry Applications. 1985;IA-21(5):1136–44.

[31] Hu Y, Song X, Cao W, Ji B. New SR drive with integrated charging capacity for plug-in hybrid electric vehicles (PHEVs). IEEE Transactions on Industrial Electronics. 2014;61(10):5722–31.

[32] Holtz J. Sensorless control of induction motor drives. Proceedings of the IEEE. 2002;90(8):1359–94.

[33] Holtz J. Sensorless control of induction machines—with or without signal injection? IEEE Transactions on Industrial Electronics; 2006;53(1):7–30.

[34] Wu S, Reigosa DD, Shibukawa Y, Leetmaa MA, Lorenz RD, Li Y. Interior permanent-magnet synchronous motor design for improving self-sensing performance at very low speed. IEEE Transactions on Industry Applications. 2009;45(6):1939–46.

[35] Chau KT. Switched Reluctance Motor Drives. Electric Vehicle Machines and Drives Design, Analysis and Application: Wiley-IEEE Press; © 2015 John Wiley & Sons Singapore Pte. Ltd. p. 108–46.

[36] Fahimi B, Suresh G, Ehsani M, editors. Review of sensorless control methods in switched reluctance motor drives. In: 2000 Conference Record of the 2000 IEEE Industry Applications Conference; 2000.

[37] Pyrhonen J, Jokinen T, Hrabovcova V. Design of Rotating Electrical Machines. 2nd ed: Wiley; Chichester, West Sussex, PO19 8SQ, United Kingdom; 2013.

[38] Krishnan R, Arumugan R, Lindsay JF. Design procedure for switched-reluctance motors. IEEE Transactions on Industry Applications. 1988;24(3):456–61.

[39] Nakao N, Akatsu K, editors. A simple unipolar excitation strategy for switched reluctance motors by using PWM current control. In: 2013 IEEE ECCE Asia Downunder (ECCE Asia); 2013 3–6 June 2013.

[40] Jeyabharath R, Veena P, Rajaram M, editors. A novel DTC strategy of torque and flux control for switched reluctance motor drive. In: 2006 PEDES '06 International Conference on Power Electronics, Drives and Energy Systems; 2006 12–15 Dec. 2006.

[41] Kioskeridis I, Mademlis C. Maximum efficiency in single-pulse controlled switched reluctance motor drives. IEEE Transactions on Energy Conversion. 2005;20(4):809–17.

[42] Schaltz E. Chapter 1. Electrical Vehicle Design and Modeling. Electric Vehicles—Modelling and Simulations: InTech; 2011. p. 1–24.

[43] Pacejka HB. Tyre and Vehicle Dynamics: Butterworth-Heinemann. The Boulevard, Langford Lane, Oxford OX5 1GB, UK; 2006.

[44] Lee D-H. Advanced torque control scheme for the high speed switched reluctance motor. In: Ahmad M, editor. Advances in Motor Torque Control: InTech; 2011. p. 87–114.

[45] Moreno-Torres P, Blanco M, Lafoz M, Arribas J. Educational project for the teaching of control of electric traction drives. Energies. 2015;8(2):921.

[46] Carstensen C. Eddy Currents in Windings of Switched Reluctance Machines. Christian Carstensen 2007 http://publications.rwth-aachen.de/record/49862/files/Carstensen_Christian.pdf.

[47] Barbisio E, Fiorillo F, Ragusa C. Predicting loss in magnetic steels under arbitrary induction waveform and with minor hysteresis loops. IEEE Transactions on Magnetics. 2004;40(4):1810–19.

[48] Miller TJE. Switched Reluctance Motors and their Control. 2nd ed: Magna Physics Publications. Oxford, England; 1993.

[49] Calverley SD, Jewell GW, Saunders RJ. Aerodynamic losses in switched reluctance machines. IEE Proceedings: Electric Power Applications. 2000;147(6):443–48.

[50] Grbovic PJ. Interfase DC-DC Converters. Ultra-Capacitors in Power Conversion Systems: Analysis, Modeling and Design in Theory and Practice: Wiley-IEEE Press. Chichester, West Sussex, PO19 8SQ, United Kingdom; 2013. p. 216–316.

[51] Wintrich A, Nicolai U, Tursky W, Reimann T. Application Manual Power Semiconductors Dr.-Ing. Arendt Wintrich Dr.-Ing. Ulrich Nicolai Dr. techn. Werner Tursky

Univ.-Prof. Dr.-Ing. Tobias Reimann Published by SEMIKRON International GmbH, Germany ISBN 978-3-938843-83-3 2nd revised edition https://www.semikron.com/dl/service-support/downloads/download/semikron-application-manual-power-semiconductors-english-en-2015 2011.

[52] ABB Switzerland Ltd. Thermal runaway during blocking Application Note 5SYA 2045-01 ABB Switzerland Ltd Semiconductors https://library.e.abb.com/public/4839b96959e24e32b59b08285a11bff0/Thermal%20runaway%20during%20blocking_5SYA%202045-01NLay.pdf 2013.

[53] Torkaman H, Afjei E. Sensorless method for eccentricity fault monitoring and diagnosis in switched reluctance machines based on stator voltage signature. IEEE Transactions on Magnetics. 2013;49(2):912–20.

[54] Marques JF, Estima JO, Gameiro NS, Cardoso AJM. A new diagnostic technique for real-time diagnosis of power converter faults in switched reluctance motor drives. IEEE Transactions on Industry Applications. 2014;50(3):1854–60.

[55] Yihua Hu CG, Wenping Cao and Stephen Finney. Fault diagnosis of switched reluctance motors in electrified vehicle applications. In: Chomat M, editor. New Applications of Electric Drives: InTech; 2015. p. 59–86.